V15

Characterization of silicon strip sensors

Theodor Zies
theodor.zies@tu-dortmund.de

Can Toraman
can.toraman@tu-dortmund.de

Measurements: 19.04.2024

Hand-in: xx.xx.2024

TU Dortmund – Physics department

Contents

1 Theorie

test cock [2]

2 Durchführung

3 Analysis

As a first step all of the aquired *.h5* data is converted into *.txt* files with the help of the provided *execute.py* script.

3.1 Depletion voltage

The first part of the analysis is the measurement of the current-voltage characteristic of the silicon strip sensor. In Figure 1, the measured leakuge current is displayed with the corresponding applied bias voltage. A flattening of the curve at $60\,\text{V}$ is cleary visible, this corresponds exactly to the depletion voltage $U_\text{dep} = 60\,\text{V}$ of the chip stated by the manufacturer. For the following measurements, the bias voltage is set to $80\,\text{V}$ to ensure the chip is always fully depleted.
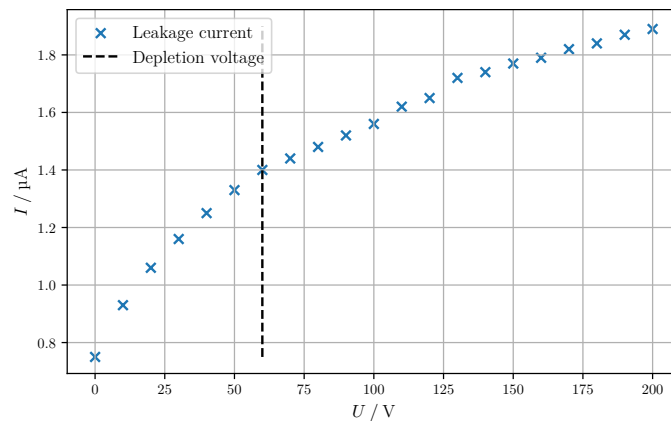

Figure 1: Plot of the measured current-voltage characteristic.

3.2 Pedestal run

Next, the pedestal run is evaluated to determine the noise of the strips. The pedestal for each strip is calculated by taking the mean value of the ADC counts of all events for each individual strip, as given by (**??**). The common mode shift for each event is then aquired by substracting the pedestal from the ADC counts of each strip and again taking the mean value according to (**??**). At last, the noise is determined using the previous results by plugging them into (**??**). A bar diagram of the pedestals and noise is shown in Figure 2.
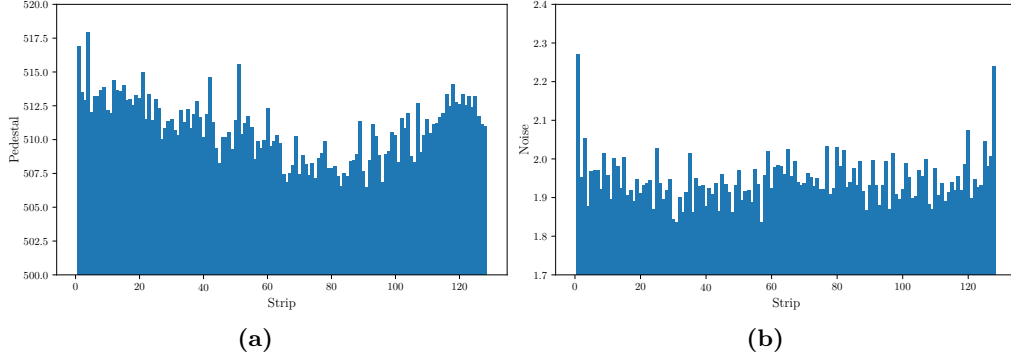
Figure 2: Bar diagrams of the pedestals (a) and noise (b) of the 128 individual strips.

The diagrams show a visible increase of the pedestals and noise towards the edges of the chip, this might have something to with the structure of the chip or the way the signal is read out. A histogram of the common mode shift is displayed in Figure 3.
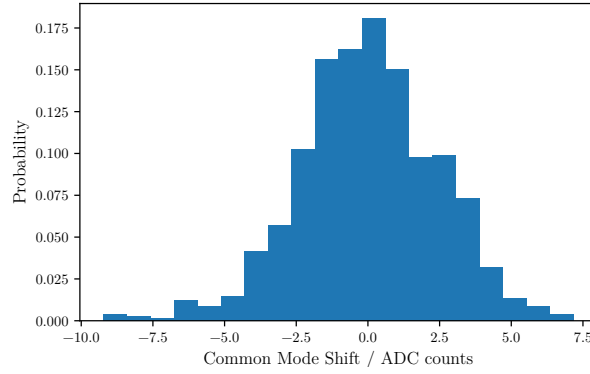

Figure 3: Commong mode shift measured during the pedestal run.

As expected, the common mode shift also referred to as *common noise* follows a gaussian distribution around 0.

3.3 Calibration measurements

Next, the data aquired from the calibration run is analysed. The results from the delay measurement are shown in Figure 4.
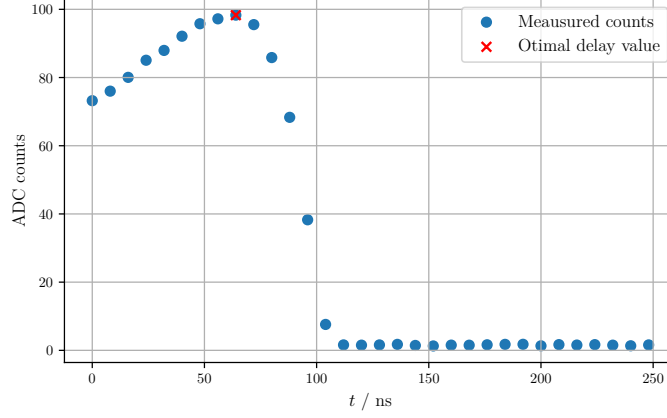
Figure 4: Results from the delay measurement.

Figure 4 shows the ADC counts depending on the delay of the laser. The highest counts were archieved at 64 ns, which is why this value was set as the laser delay for the rest of the experiment. After this, a calibration curve is measured for five different channels. This curve gives the relation between the injected charge and the ADC counts. The five curves are given in Figure 5a. Additionally for channel 60, a curve at 0 V is recorded, it can be seen in Figure 5b, where it is compared to the regular curve of channel 60.
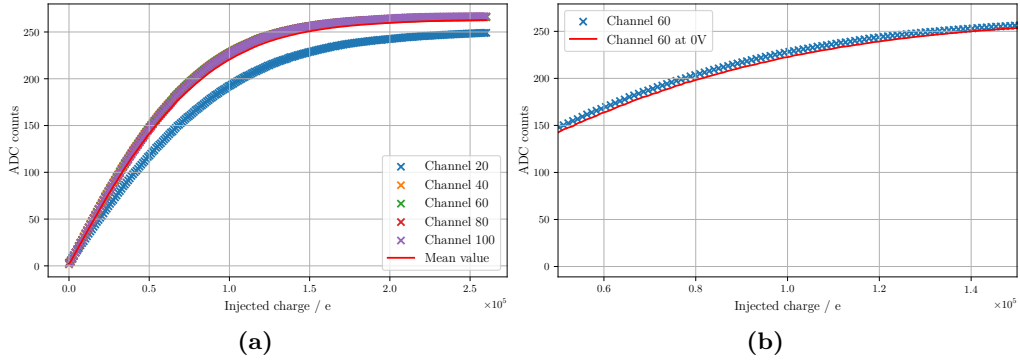

| (a) | (b) |

Figure 5: Calibration curve of five channels (a) and detailed view of channel 60 at 0 V (b).

As seen in Figure 5a, all channels show almost exactly the same calibration curve. For some unknown reason, channel 20 meausured significantly less ADC counts. For the next step, the mean value of the five channels is taken. The calibration curve at 0 V is very similar to the one measured above the depletion voltage. This leads to the conclusion that the relation between the ADC counts and the injected charge does not depend on the applied bias voltage. To further quantify this dependecy of the counts and the injected charge, a 4-th degree polynomial is fit to the mean counts of the five channels. The polynomial is of the from

$$Q(\mathrm{ADC}) = a \cdot \mathrm{ADC}^4 + b \cdot \mathrm{ADC}^3 + c \cdot \mathrm{ADC}^2 + d \cdot \mathrm{ADC} + e \,. \tag{1}$$

The fit is performed using the *curvefit* method from the *scipy* [3] package. The result is shown in Figure 6, the fit range is restricted to the range below 250 ADC counts to get a good result.
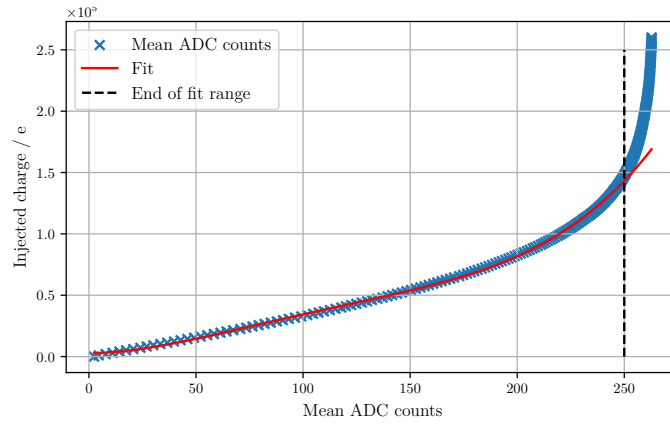

Figure 6: Fit of 4-th degree polynomial to the mean ADC counts of the calibration run.

The fit yields the following coefficients for (1)

$$a = (0{,}000\,111 \pm 0{,}000\,006)\,\mathrm{e}$$
$$b = (-0{,}0439 \pm 0{,}0032)\,\mathrm{e}$$
$$c = (6{,}2 \pm 0{,}6)\,\mathrm{e}$$
$$d = (30 \pm 40)\,\mathrm{e}$$
$$e = (2600 \pm 700)\,\mathrm{e}\,.$$

These coefficients together with (1) now allow any ADC counts to be converted into an electric charge.

3.4 Measuring the strip sensor by using the laser

The physical structure of the sensor and its strips is determined by using the laser. Before the measurement can be started, the optimal delay between laser signal and chip readout is determined by plotting the data from the *Laser Sync* run. This is shown in Figure 7, where it is cleary visible that the maxiaml ADC counts are archieved at a delay of 100 ns.
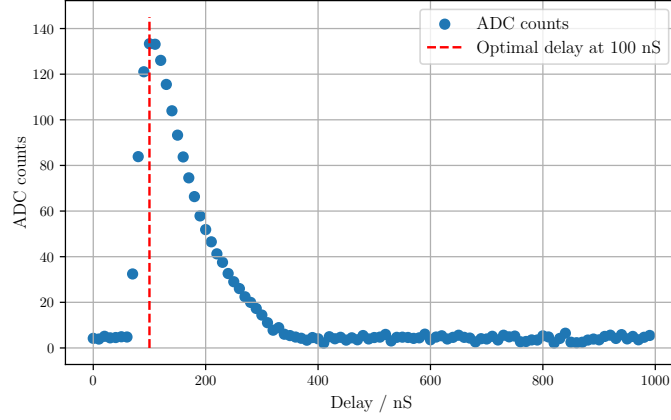
Figure 7: Results of the *Laser Sync* run.

After moving the laser across the 35 µm intervall, a heatmap is produced showing the signal of the relevant channels that were hit by the laser. Figure 8 shows the affected channels 82-85 and their signal strength depending on the laser position.
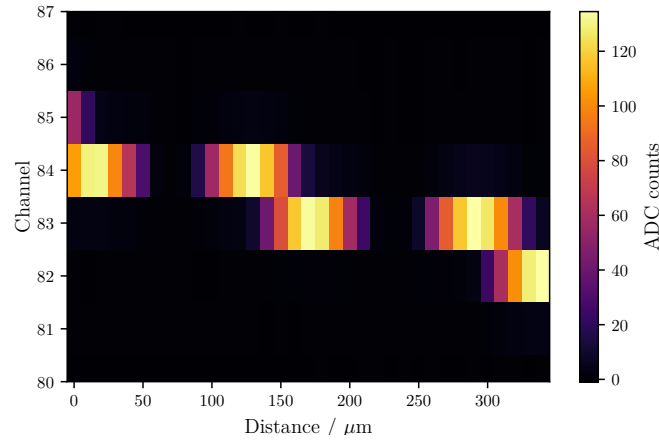

Figure 8: Heatmap of the signal strength of the affected channels depending on the laser position.

In the following, the individual signal for channel 83 is analysed in Figure 9. The position of the beginning, peak and end of the signal is also shown.
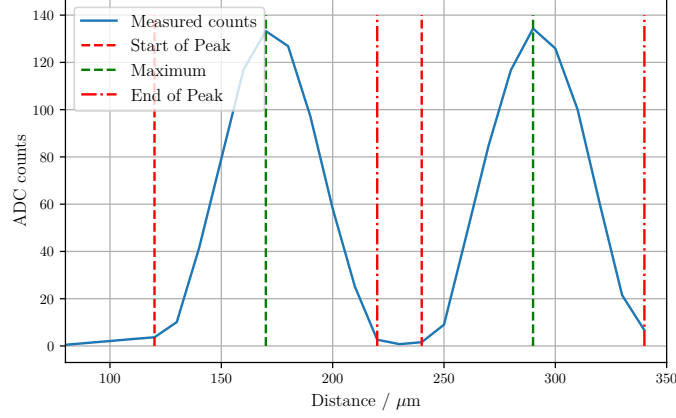
Figure 9: Signal strength of channel 83 depending on the laser position.

The width of the strip is simply the distance between the two peaks, as this is the position where the laser is on the channel but reflected by the metal of the strip. The extension of the laser can be estimated by the distance between the start of a peak and its maximum. All relevant positions are marked in Figure 9 and the resulting values are

$$\text{width of strips} = 290 \, \mu\text{m} - 170 \, \mu\text{m} = 120 \, \mu\text{m}$$
$$\text{laser extension} = 170 \, \mu\text{m} - 120 \, \mu\text{m} = 50 \, \mu\text{m} \, .$$

The distance of two strips can be determined by comparing the position of the maxima of two different channels in Figure 8

$$\text{distance} = 40 \, \mu\text{m} \, .$$

The pitch is then calculated as the sum of the distance between the strips and their width

$$\text{pitch} = 120 \, \mu\text{m} + 40 \, \mu\text{m} = 160 \, \mu\text{m} \, .$$

3.5 Determination of the charge collection efficiency

The charge collection efficiency of the laser is determined by measuring the relation between the collected charge (ADC counts) and the applied bias voltage.

3.5.1 Using the laser

When using the laser, at first the channel on which the laser is focused during the measurement is to be determined. By plotting a heatmap of the ADC counts for each channel, Figure 10 cleary shows that the laser was focused on channel 73.
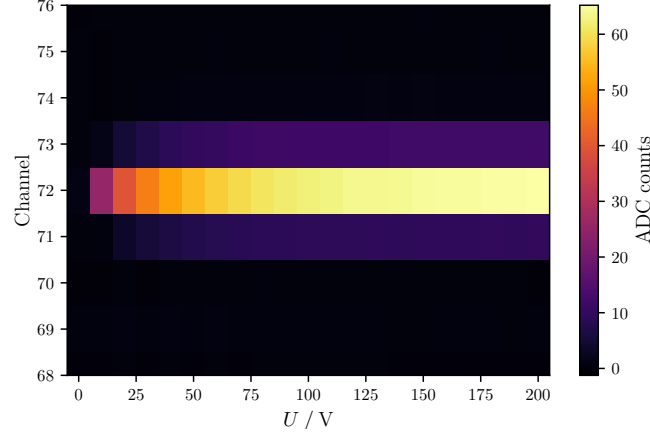
8

Figure 10: Heatmap showing the ADC counts of each channel and bias voltage.

Thus in the following, only the data from channel **73** is considered. In order to get the charge collection efficiency, the measured ADC counts have to be normalized in regard to the maximum ADC counts of the plateu. In theory, the plateu should show constant counts after the depletion voltage U_{dep} is reached, however the acutal data shows a slight increase in this area. This is why the counts are normalized in regard to the first value of the plateu, so that a proper fit of (**??**) can be performed. The normalized counts in dependence of the bias voltage are shown in Figure 11.
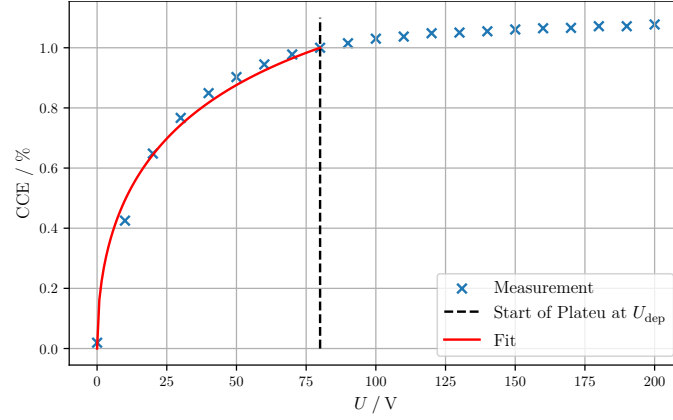

Figure 11: Charge collection efficiency of channel 73.

The fit was performed in the range $0\,\mathrm{V} < U < 80\,\mathrm{V}$. The depletion voltage of $U_{\mathrm{dep}} = 80\,\mathrm{V}$ is a fixed paramter in (**??**), whereas the value of the penetration depth a of the laser is determined via the fit as

$$a = (253 \pm 6)\,\mathrm{\mu m}\,.$$

9

3.5.2 Using the beta source

The same curve is now measured by replacing the laser as a source with a β^- source. The ADC counts are now determined in clusters. To get the charge collection efficiency, the entries in each cluster are summed, after this the mean value of all clusters is taken. A normalization is performed analogously to the one of laser measurement. The resulting curve is displayed in Figure 12.
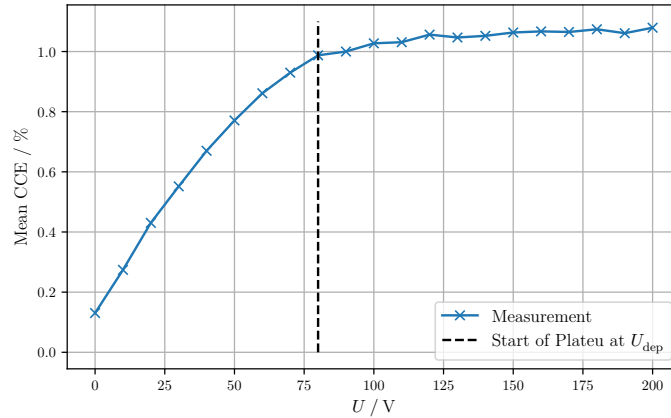

Figure 12: Charge collection efficiency determined via the β^- source.

3.6 Large source scan

Finally, the large source scan containing roughly one million events is analysed. Figure 13 shows how the number of cluster per event is distributed as well as how many channels exist per cluster.
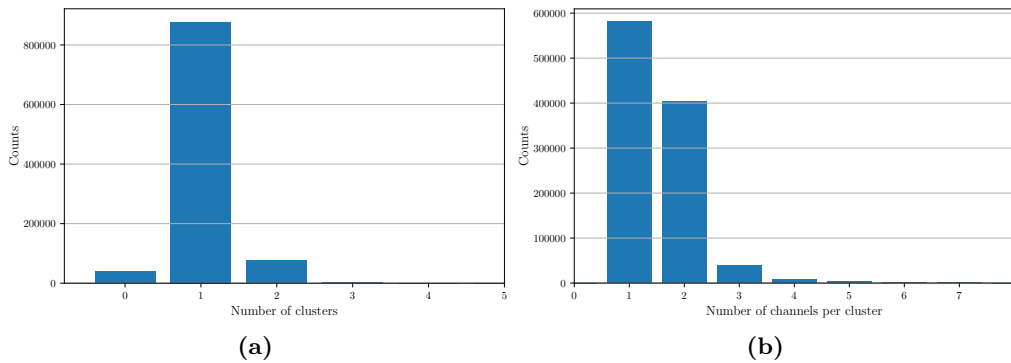

Figure 13: Number of clusters per event (a) and number of channels per cluster (b).

Next, a hitmap is produced for all channels. This is displayed in Figure 14 and shows how many events/hits were registered by each individual channel. An events mostly leads to the formation of one cluster, and each cluster usually contains the signal of one to three channels.
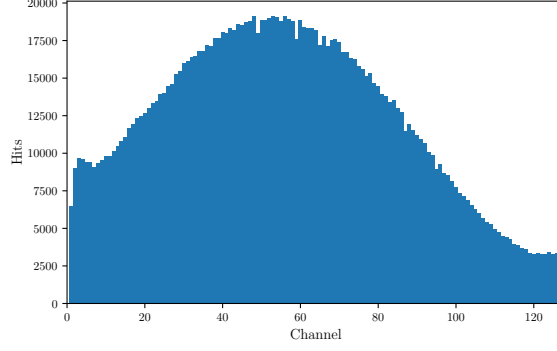
Figure 14: Hitmap displaying the events of each channel.

Most of the hits are registered in the middle of the chip, while the edges cleary show a lower amount of entries. Lastly, the distribution of the measured ADC counts as well as the energy spectrum is computed. To aquire the energy spectrum from the ADC counts, the counts are converted into an electric pulse with the conversion formula (1) determined during the calibration run. The pulse is then converted into an energy by using the fact that the energy needed to generate an electron-hole pair is approximatly $3,6\,\mathrm{eV}$ [1]. Figure 15 shows both distributions.
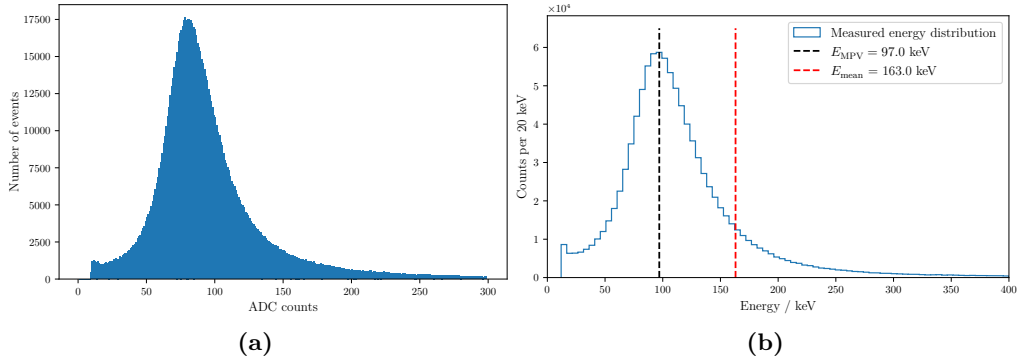

Figure 15: Distribution of the ADC counts (a) and the energy (b).

The distribution of the energ spectrum allows to determine the most probable energy and mean energy of the β^- source as

$$E_{\mathrm{MPV}} = 97\,\mathrm{keV}$$
$$E_{\mathrm{Mean}} = 163\,\mathrm{keV}\,.$$

4 Discussion

References

[1] *V15-Characterization of silicon strip sensors.* TU Dortmund, Department of physics.

[2]   *Versuch zum Literaturverzeichnis*. TU Dortmund, Fakultät Physik. 2022.

[3]   Pauli Virtanen et al. "SciPy 1.0: Fundamental Algorithms for Scientific Computing in Python". In: *Nature Methods* 17 (2020), pp. 261–272. DOI: 10.1038/s41592-019-0686-2.